Valence Tautomerism in One Dimensional Coordination Polymers

Olga Drath,[†] Robert W. Gable,[†] Boujemaa Moubaraki,[‡] Keith S. Murray,[‡] Giordano Poneti,[§,≠] Lorenzo Sorace[§] and Colette Boskovic*[†]*

[†] School of Chemistry, University of Melbourne, Victoria, 3010, Australia.

[‡] School of Chemistry, Monash University, Clayton, 3800, Australia

[§] UdR INSTM and Department of Chemistry "U. Schiff", University of Florence, 50019 Sesto Fiorentino (FI), Italy.

[≠] Current address: Instituto de Química, Universidade Federal do Rio de Janeiro, 21941-909 Rio de Janeiro, Brazil

* c.boskovic@unimelb.edu.au & lorenzo.sorace@unifi.it

RECEIVED DATE (to be automatically inserted after your manuscript is accepted if required according to the journal that you are submitting your paper to)

The combination of the divergent bis-pyridyl linking ligands 1,2-bis(4-pyridyl)ethane (1,2-bpe), 4,4'-*trans*-azopyridine (azpy) and 1,3-bis(4-pyridyl)propane (1,3-bpp) with cobalt and 3,5-di-*tert*-butyldioxolene (3,5-dbdiox) ligands has afforded the complexes [Co(3,5-dbdiox)$_2$(1,2-bpe)] (**1**), [Co(3,5-dbdiox)$_2$(azpy)] (**2**), [*trans*-Co(3,5–dbdiox)$_2$(1,3-bpp)] (**3a**) and [*cis*-Co(3,5-dbdiox)$_2$(1,3-bpp)] (**3b**). All species are 1D coordination polymers that crystallize as solvated forms; geometric isomers **3a** and **3b** co-crystallize. Complexes **1**, **2** and **3a** exhibit around the Co centers a *trans* disposition of the N-donor atoms from the pyridyl linkers, while an unusual *cis* disposition is evident in **3b**. Single crystal X-ray structural analysis at 100 or 130 K of solvated forms of these complexes indicate that all complexes possess the {Co^{III}(3,5-dbcat)(3,5-dbsq)} (3,5-dbcat = 3,5-di-*tert*-butylcatecholate; 3,5-dbsq = 3,5-di-*tert*-butyl-semiquinonate) charge distribution at the temperature of data collection. Variable temperature magnetic susceptibility studies indicate that **1**, **1**·1.5MeCN·2H$_2$O, **2**·2EtOH and **3**·MeCN·H$_2$O (**3** = **3a**·**3b**) all exhibit thermally induced valence tautomeric (VT) transitions above 200 K. Multiple heating and cooling cycles indicate that the behavior in some cases is strongly dependent on desolvation processes. Most notably, further desolvation of **1**·1.5MeCN·2H$_2$O, above 340 K affords $\chi_m T$ values that suggest unusual ferromagnetic coupling in the {*hs*-Co^{II}(3,5-dbsq)$_2$} valence tautomer. Compound **3**·MeCN·H$_2$O exhibits a two-step VT transition that may be ascribed to the presence of the *cis* and *trans* geometric isomers. Compounds **1**, **1**·1.5MeCN·2H$_2$O, **2**·2EtOH and **3**·MeCN·H$_2$O all also exhibit a single photo-induced VT transition, comparable to those generally observed for non-polymeric cobalt-dioxolene complexes.

INTRODUCTION

With a view towards the miniaturization of electronic devices, the last two decades have seen the development of molecular materials that can be switched between distinguishable electronic states upon application of an appropriate external stimulus, including spin crossover (SCO) and valence tautomeric

(VT) compounds.[1,2] Due to significant changes in optical and/or magnetic properties associated with the intramolecular electron transfer and/or spin transitions, these materials are of interest for data storage, sensors, display devices and molecular electronics. Valence tautomerism involves electron transfer between a redox-active metal cation and a redox-active ligand.[3-6] Since the first report in 1980,[7] a number of octahedral cobalt complexes with redox-active 3,5-di-*tert*-butyldioxolene (3,5-dbdiox) ligands and N-donor ancillary ligands have been found to undergo both thermally - and light-induced - VT transitions. For these complexes, electron transfer between the cobalt cation and 3,5-dbdiox ligand is accompanied by a metal-based spin transition such that the complexes switch between low spin Co(III)-catecholate {*ls*-Co^{III}(3,5-dbcat)} and high spin Co(II)-semiquinonate {*hs*-Co^{II}(3,5-dbsq)} forms.

In addition to exhibiting a reversible electronic transition, molecular materials for use in devices should ideally also display abrupt transitions and hysteresis that gives rise to bistability. These characteristics can be accessed in cooperative systems, in which the electronic state changes are propagated throughout the crystal lattice. Already observed for SCO materials,[8,9] higher cooperativity has been realised by a combination of short-range[10-12] and long-range interactions.[13] In particular, considerable progress has been achieved with spin crossover coordination polymers (SCO CPs),[14–18] which can inform the design of analogous VT coordination polymers (VT CPs). Of most relevance to the design of new VT CPs are 1,2,4-triazole based 1D SCO CPs, which have been the subject of intensive studies oriented towards transferring the SCO properties to technologically convenient platforms such as composites and gels,[19] liquid-crystalline materials,[20] dendrimers,[21] Langmuir-Blodgett films[22] and nanoparticles.[23-25] In some cases, these materials display abrupt and hysteretic thermally-induced transitions near room temperature, making them attractive candidates for memory and sensors applications.[26,27] Extending the synthetic approach to divergent bi- and polydentate pyridine-like bridges has afforded 2D and 3D SCO CPs.[28-33]

While most VT complexes are mononuclear, some 1D VT CPs have been reported. The first of these was $[Co(pyz)(3,6\text{-dbdiox})_2]_\infty$ (pyz = pyrazine, 3,6-dbdiox = 3,6-di-*tert*-butyldioxolene), which undergoes a thermally-induced VT transition, but does not show a photoinduced transition at low

temperature.[34] Following a different strategy, Dei and coworkers subsequently reported the formation of a 1D CP constructed from {Co-(1,10-phenanthroline)} units linked via a ditopic bridging dioxolene ligand, which exhibits a VT transition that can be photoinduced and shows a 12 K wide thermal hysteresis around room temperature.[35,36] Ruiz-Molina *et al.* used 4,4'-bipyridine (4,4'-bpy) and 1,4-bis(imidazol-1-ylmethyl)benzene (bix) to link {Co(3,5-dbdiox)$_2$} units building blocks into similar 1D VT CPs and VT nanoparticles.[37] More recently, the same group reported a new VT CP using a multitopic ligand that combines a catechol and a pyridine unit, although the dimensionality of the CP was not established.[38] Another N-donor linking ligand - meso-alpha,beta-di(4-pyridyl)glycol (dpg) - was used by Tao *et al.* to synthesise a "*cis"* 1D zig-zag chain, which undergoes thermal, pressure and light induced VT intraconversion.[39] The same group reported three 1D VT complexes containing Co-dioxolene units connected by exo-bidentate pyridine ligands: 1,2-bis(4-pyridyl)ethylene, *trans*-4,4'-azopyridine and 1,4-bis(4-pyridyl)benzene, one of which displays thermal and light-induced VT transitions.[40] These compounds also exhibit a strong dependence of the nature of the VT transition on the solvation of the compound, as has been observed previously for non-polymeric VT complexes.[36-38, 41] Finally, Sato and co-workers have very recently reported a thermally-induced VT transition for 1D cobalt-dioxolene CP with 4,4'-bipyridyl ligands linking cobalt bis-dioxolene units with chiral dioxolene ligands.[42]

In search of new CPs that undergo VT transitions, we employed the divergent bis-pyridyl ligands (Chart 1) 1,2-bi(4-pyridyl)ethane (1,2-bpe), *trans*-4,4'-azopyridine (azpy) and 1,3-bis(4-pyridyl)propane (1,3-bpp) to link {Co(3,5dbdiox)$_2$} units. Herein we report the synthesis and structural, electronic and (photo-)magnetic properties of the systems obtained using this strategy.

Chart 1. Bis-pyridyl ligands used in this study.

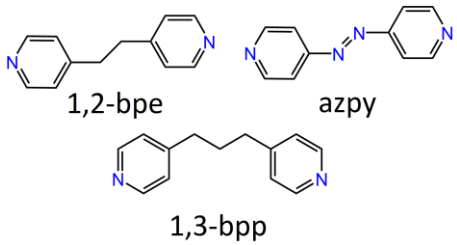

EXPERIMENTAL SECTION

Synthesis. All the reagents, excluding azpy, were obtained from commercial sources and were used as received. The azpy ligand was synthesized according to the literature procedure.[43]

[Co(3,5-dbdiox)$_2$(1,2-bpe)]$_\infty$ (1). *Method 1.* An ethanol solution (3.75 ml) of 3,5-dbcatH$_2$ (33 mg, 0.15 mmol) and 1,2-bpe (14 mg, 0.075 mmol) was layered over an aqueous solution (3ml) of Co(OAc)$_2$·4H$_2$O (19 mg, 0.075 mmol). The ethanol and water layers were separated by a buffer layer of ethyl acetate (1 ml). After 5 days blue rectangular plate-shaped crystals were formed. A sample for single crystal X-ray diffraction was maintained in contact with the mother liquor to avoid solvent loss and identified as **1**·2 H$_2$O. The product was isolated by filtration, washed with cold ethanol and air dried, giving a desolvated sample of **1** in 30% yield. Anal. Calcd (%) for $C_{40}H_{52}O_4CoN_2$ (**1**): C, 70.3; H, 7.8; N, 4.1. Found: C, 70.1; H, 7.7; N, 4.2. Selected IR (cm^{-1}): 2952 (vs), 1615 (s), 1580 (m), 1503 (w), 1464 (vs), 1387 (m), 1356 (s), 1284 (m), 1245 (m), 1209 (m), 1095 (m), 1070 (m), 1035 (m), 986 (s), 827 (m), 551 (w). Thermogravimetric analysis confirmed the absence of solvation for **1**.

Method 2. Complex **1** was synthesised adapting the method reported previously by Tao *et al.* with other ligands.[40] An acetonitrile solution (6.7 ml) of 3,5-dbcatH (15 mg, 0.067 mmol) and 1,2-bpe (12mg, 0.067mmol) was layered over an aqueous solution (1.3 ml) of Co(OAc)$_2$·4H$_2$O (17 mg, 0.067 mmol). Green rectangular plate-shaped crystals were obtained after several weeks. A crystal suitable for single crystal X-ray diffraction was maintained in the mother liquor and identified as **1**·2MeCN·2H$_2$O. The product was isolated by filtration, washed with acetonitrile and air dried, affording partially desolvated **1**·1.5MeCN·2H$_2$O in 20% yield. Anal. Calcd (%) for $C_{43}H_{60.5}N_{3.5}O_6Co$ (**1**·1.5MeCN·2H$_2$O):

C, 66.1; H, 7.8; N, 6.3. Found: C, 65.7; H, 7.6; N, 6.3. Selected IR (cm^{-1}): 2953 (vs), 1616 (s), 1578 (m), 1463 (vs), 1387 (m), 1357 (s), 1287 (m), 1243(m), 1206(m), 1095(m), 1067(m), 1027(m), 984(s), 838(m), 555(m). Applying the method Tao *et al.* employed to desolvate related compounds,[40] vacuum drying **1**·1.5MeCN·2H_2O at 90 °C afforded samples that were very hygroscopic, with elemental and thermogravimetric analysis suggesting adsorption of several water molecules per formula unit upon exposure of the vacuum-dried sample to air.

[Co(3,5-dbdiox)$_2$(azpy)]$_\infty$ (2). This complex was synthesized according to method 1 used for complex **1**, with replacement of 1,2-bpe with azpy (14 mg, 0.075 mmol) to afford green rectangular plate-shaped crystals. A sample for single crystal X-ray diffraction was maintained in the mother liquor to avoid the solvent loss and identified as **2**·2EtOH. The product was isolated by filtration, washed with cold ethanol and air dried, giving a sample of **2**·2EtOH in 18% yield. Anal. Calcd (%) for $C_{42}H_{60}N_4O_6Co$ (**2**·2EtOH): C, 65.0; H, 7.8; N, 7.2. Found: C, 64.9; H, 7.2; N, 7.1. Selected IR (cm^{-1}): 2956 (vs), 1600 (s), 1582 (m), 1459 (vs), 1387 (m), 1356 (s), 1288 (m), 1246 (m), 1201 (m), 1097 (m), 1052 (m), 1027 (m), 986 (s), 855 (m), 574 (m). Vacuum drying **2**·2EtOH at 90 °C appears to cause decomposition, affording material, for which even an approximately good fit of the elemental analysis cannot be found.

{[*trans*-Co(3,5-dbdiox)$_2$(1,3-bpp)]$_\infty$·[*cis*-Co(3,5-dbdiox)$_2$(1,3-bpp)]$_\infty$} (3). This compound was synthesized according to method 2 used for complex **1**, with replacement of the 1,2-bpe ligand with 1,3-bpp (0.15 mg, 0.067 mmol). Blue rectangular plate-shaped crystals were obtained after several weeks. A crystal for single crystal X-ray diffraction was maintained in the mother liquor and identified as a **3**·2MeCN·H_2O. The product was isolated by filtration, washed with acetonitrile and air dried, giving a partially desolvated sample of **3**·MeCN·H_2O in 30% yield. Anal. Calcd (%) for $C_{84}H_{103}O_9Co_2N_5$ (**3**·MeCN·H_2O): C, 69.4; H, 7.8; N, 4.8. Found: C, 69.1; H, 7.9; N, 4.7. Selected IR (cm^{-1}): 2953 (vs), 1616 (s), 1580 (m), 1503 (w), 1477 (vs), 1445 (vs) 1387 (m), 1356 (s), 1284 (m), 1246 (m), 1208 (m), 109 5(m), 1069 (m), 1018 (m), 986 (s), 856 (m), 496 (w).

Single Crystal X-Ray Data Collection and Structure Solution. The crystallographic data (Table 1) for compounds **1**·2H_2O and **1**·2MeCN·2H_2O were collected at 130 K on an Agilent Technologies SuperNova diffractometer using CuKα radiation. Data for compounds **2**·2EtOH and **3**·2MeCN·H_2O were collected at 100 K, using MoKα radiation, on the MX1 and MX2 beamlines, respectively, at the Australian Synchrotron, Victoria, Australia. Using OLEX2[44], all the structures were solved with the ShelXT[45] structure solution program using direct methods and refined with the ShelXL refinement package using least squares minimization. Compounds **1**·2H_2O, **2**·2EtOH, **3**·2MeCN·H_2O contained disordered solvent. A satisfactory disorder model of the solvent could not be not found, and therefore the OLEX2 Solvent Mask routine was used to mask out the disordered electron density. [46] The molecular formulas proposed are based on the calculated solvent accessible voids and the electron count, as well as the elemental and thermogravimetric analysis for the dried samples. All attempts to collect data for **3**·2MeCN·H_2O suggested minor twinning of the crystals; a twin refinement was successfully carried out using the collected data.

Table 1. Crystallographic data for **1**·2H_2O, **1**·2MeCN·2H_2O, **2**·2EtOH and **3**·2MeCN·H_2O

	1·2H_2O	**1**·2MeCN·2H_2O	**2**·2EtOH	**3**·2MeCN·H_2O
Formula	$C_{40}H_{56}N_2O_6Co$	$C_{44}H_{62}N_4O_6Co$	$C_{42}H_{60}N_4O_6Co$	$C_{86}H_{116}Co_2N_6O_9$
Formula weight / g mol^{-1}	719.79	801.90	775.88	1495.74
Crystal system	Monoclinic	Triclinic	Monoclinic	Monoclinic
Space group	*I*2/*a*	$P\bar{1}$	$P2_1/n$	$P2_1/n$
a / Å	10.3003(2)	8.5243(5)	14.642(3)	11.817(2)
b / Å	26.4541(5)	11.2051(7)	10.495(2)	25.188(5)
c / Å	32.4520(9)	11.8539(7)	28.554(6)	27.794(6)
α	90	104.689(5)	90	90
β	94.965(2)	96.320(5)	97.42(3)	94.40(3)
γ	90	97.765(5)	90	90

V / Å^3	8809.5(4)	1072.8(1)	4351(2)	8248(3)
Z	8	1	4	4
T / K	130	130	100	100
ρ_{calc} / g cm^{-3}	1.085	1.241	1.184	1.190
μ / mm^{-1}	3.378	3.534	0.442	0.459
Reflns measd	33084	9132	51165	140147
Unique reflns	9186	4466	7109	18779
Data / restraints / parameters	9186 / 43 / 364	4466 / 0 / 260	7109 / 30 / 472	18779 / 46 / 955
R_{int}	0.1030	0.0310	0.0974	0.0879
R_1 [$I > 2\sigma(I)$]	0.0954	0.0547	0.0800	0.0906
wR_2 (all data)	0.3147	0.1618	0.2356	0.2768
Goodness-of-fit on F^2	1.004	1.075	1.092	1.108
$\Delta\rho_{max,min}$ / e Å^{-3}	0.93/-0.82	0.44/-0.95	1.23/-0.85	1.20/-0.80

Magnetic Measurements. Magnetization measurements were carried out using a Quantum Design MPMS SQUID magnetometer equipped with a 5 T magnet. The temperature dependence of the magnetization (M) was followed from 10 to 370 K by applying a 10 kOe field (H) from 370 to 40 K and a 1 kOe field below 40 K to reduce magnetic saturation effects. Magnetic susceptibility per mole (χ_M) was then evaluated as $\chi_M = M_M/H$. Thermal equilibrium of the samples was reached waiting 120 s after the stabilization at each temperature, resulting in an average 1.6 K min^{-1} sweep rate in heating and cooling cycles. To exclude the presence of spurious phases, a microcrystalline sample of **1**·1.5MeCN·2H_2O was tested by powder X-ray diffraction before measuring, providing a diffractogram as expected on the basis of the single crystal X-ray structure of **1**·2MeCN·2H_2O (Figure S1).

Photomagnetic Measurements. Photomagnetic measurements were carried out on pelletized samples obtained by mixing ~0.5 mg of microcrystalline powder (the actual cobalt content being evaluated by scaling the magnetic moment on that of a polycrystalline heavier sample) with KBr

powder and pressing into a pellet to facilitate light penetration. Irradiation experiments have been performed using a 532 nm laser beam with the continuous wave laser diode coupled to an optical fiber inserted in the sample space through a hollow sample rod and collimated on the sample by means of an aspheric lens, yielding a radiant power on the sample of about 2 mW cm^{-2}. Measurement of effective T_{LIESST} (LIESST = light induced excited spin state trapping) consisted of monitoring the temperature featuring a minimum in the $d(\chi_M T)/dT$ curve, after reaching the photostationary limit, having switched the laser off at 10 K and warming the sample at a rate of 0.3 K min^{-1}. Magnetic moments were corrected for the diamagnetic contribution of the KBr and the sample holder, independently measured in the same range of field and temperature as well as for the intrinsic diamagnetism of the sample by using appropriate Pascal constants.

Other Measurements. Elemental analyses were performed by the Campbell Microanalytical Laboratory, Department of Chemistry, University of Otago, New Zealand. Thermogravimetric analyses were performed on a Mettler Toledo thermal analyzer. Infrared spectra (KBr disk) were recorded on a Bruker Tensor 27 FTIR spectrometer. Ultraviolet-visible absorption diffuse reflectance spectra were measured on a Thermo Scientific-Evolution 220 UV-Visible spectrophotometer. Variable temperature powder X-ray diffraction data of desolvated **1** were acquired using a Bruker Advance D8 diffractometer (Cu-Kα radiation, 40 kV x 40 mA) equipped with a Material Research Instruments heating stage for temperature dependent measurements and a multi-channel energy dispersive detector (SOLX) - for variable temperature measurements up to 413 K. Room temperature powder X-ray diffraction data for **1**·1.5MeCN·2H_2O were acquired using a Bruker Advance New D8 Da Vinci in Bragg-Brentano configuration (Cu-Kα radiation, 40 kV x 40 mA). EPR spectra were measured using a Bruker Elyxsys E500 spectrometer equipped with a CF935 (Oxford instruments) continuous flow ^{4}He cryostat for low temperature studies. Comparisons between the intensities of absolute signals of microcrystalline powder samples of **1**·1.5MeCN·2H_2O, before and after heating at 370 K, was obtained by measuring a definite and comparable mass of the two samples (1.4 mg and 0.8 mg respectively).

RESULTS AND DISCUSSION

Syntheses. Crystalline samples of all compounds were obtained at room temperature by solvent diffusion in 10 ml sealed test tubes, using water / ethyl acetate / ethanol for **1** and **2**·2EtOH and water / acetonitrile for **1**·2MeCN·2H_2O and **3**·2MeCN·H_2O. In all cases, both ligands were dissolved in an organic solvent and carefully layered over an aqueous solution of cobalt(II) acetate, affording rectangular blue or green plate-shaped crystals of the neutral compounds after several weeks. This reaction involves aerial oxidation of the 3,5-dbcat^{2-} ligand and cobalt(II) metal center, which most likely follows ligand coordination to the relatively labile cobalt(II) ion. All compounds crystallize cleanly and can be isolated in moderate to good yield. Once formed, the crystals are completely insoluble in all common solvents. A differently solvated form of complex **2**, **2**·2MeCN·2H_2O, has been reported previously by Tao *et al*.[40]

Structure Description. Selected single crystal X-ray data for the compounds are reported in Table 1, structural representations of complexes **1**, **2** and the two independent molecules of complex **3** are available in Figure 1 and crystal packing diagrams for **1**·2H_2O, **1**·2MeCN·2H_2O, **2**·2EtOH and **3**·2MeCN·H_2O are reported in Figures 2 and 3. Asymmetric units of the compounds are presented in Figure S2. Compound **1**·2H_2O crystallizes in the monoclinic space group *I*2/*a*. The asymmetric unit contains one half of each of two independent cobalt atoms with one of two coordinated dioxolene ligands per metal center, one half of each of two independent 1,2-bpe linkers and disordered solvent. Uniquely among this set of compounds, **1**·2MeCN·2H_2O crystallizes in the triclinic space group $P\bar{1}$. The asymmetric unit contains half of the cobalt atom located on the inversion center, one dioxolene ligand, half of the linking bis-pyridyl ligand and solvent molecules. Compound **2**·2EtOH crystallizes in the monoclinic space group $P2_1/n$ with the asymmetric unit composed of one half of each of two independent Co-dioxolene units, the linking azpy ligand and disordered solvent. In these three compounds, complexes **1** and **2** form 1D chains with the pyridine linking moieties arranged with a *trans*- disposition with respect to the Co(II) (Figure 2). The differing packing arrangements give rise to

a different arrangement of cavities between the chains in which the solvent molecules reside. Compound **3**·2MeCN·H_2O, incorporating the flexible linking ligand 1,3-bpp, crystallizes in the monoclinic space group $P2_1/n$ as two independent interweaving chains, one of which (**3a**) exhibits a *trans*-disposition of the N-donor ligands in each {Co(3,5-dbdiox)$_2$} unit, while the other possesses the N-donor ligands arranged in a *cis* manner (**3b**). The mixture of two geometric isomeric forms of such 1D chains within the one compound is unprecedented. Only one previously reported chain has exhibited the *cis*-disposition of the N-donor linking ligands,[39] while the *trans* disposition has been observed in all other cases.[34,37,40] In addition to partially disordered solvent molecule, the asymmetric unit consists of two independent molecules, one for the each type of chain, each containing two dioxolene ligands and one 1,3-bpp ligand, coordinated to a cobalt center. The zig-zag *cis* chains pass alternately above and below each of the *trans* chains (Figure 3). The cavities between the chains are filled with highly disordered solvent: two water molecules and two acetonitrile molecules per two independent cobalt centers.

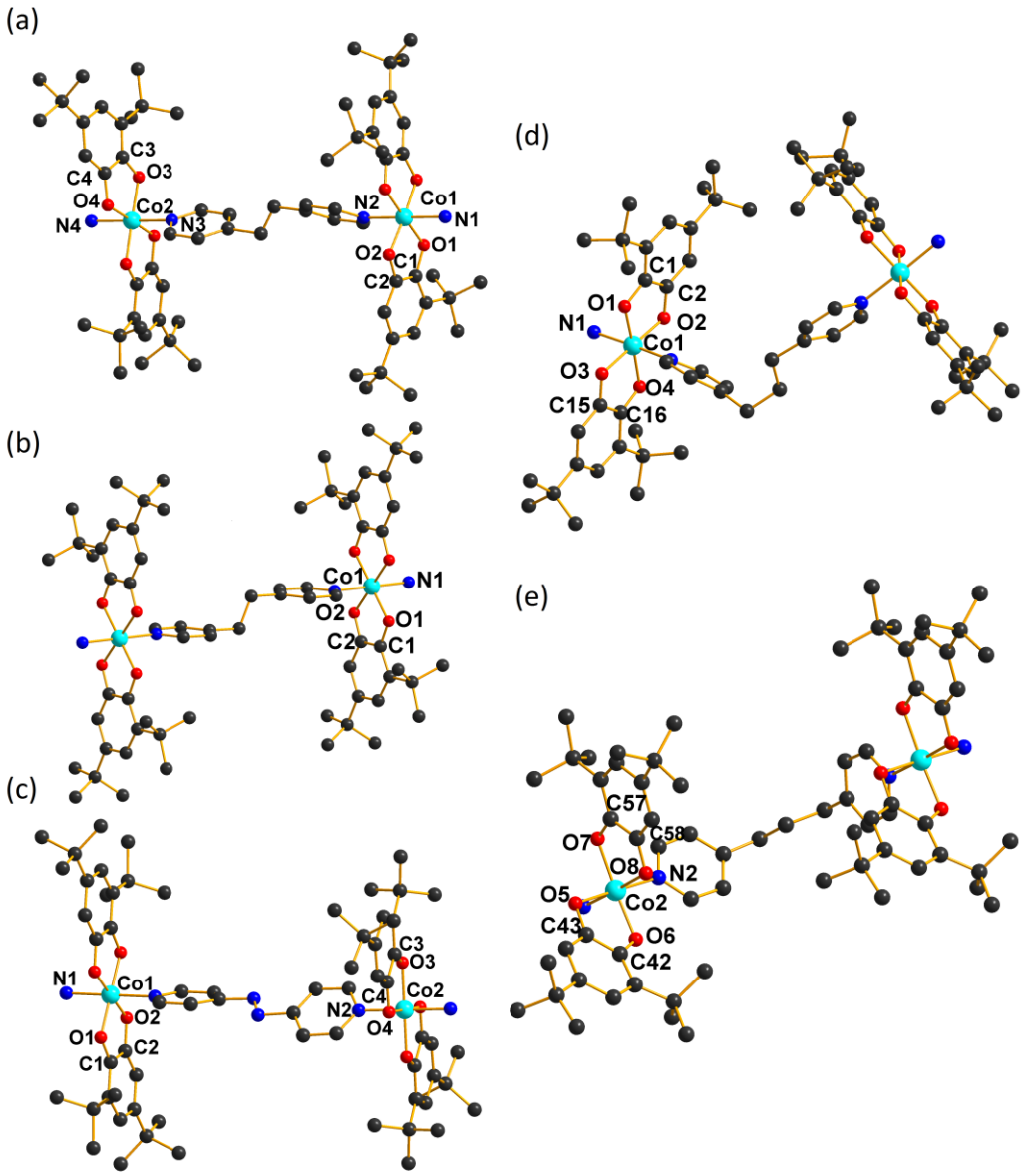

Figure 1. Structural representation of the repeat units of the 1D chain complexes (a) **1** in **1**·2H_2O, (b) **1** in **1**·2MeCN·2H_2O, (c) **2** in **2**·2EtOH, (d) *trans*-disposed **3a** in **3**·2MeCN·H_2O and (e) *cis*-disposed **3b** in **3**·2MeCN·H_2O. Color code: Co, cyan; O, red; N, blue and C, black.

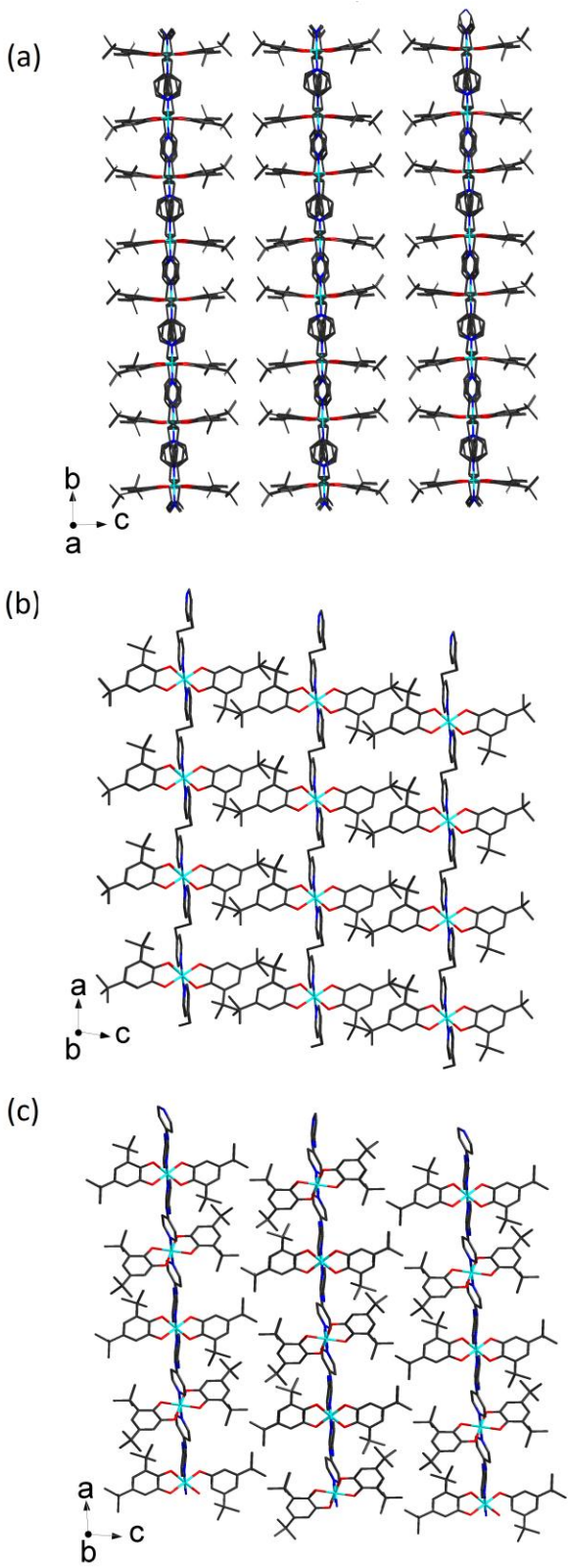

Figure 2. Crystal packing diagrams of (a) **1**·2H_2O, (b) **1**·2MeCN·2H_2O and (c) **2**·2EtOH. Color code as per Figure 1. Hydrogen atoms and solvent molecules omitted for clarity.

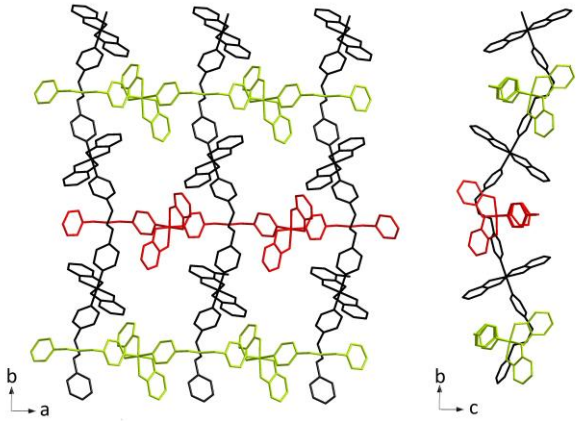

Figure 3. Crystal packing diagrams of **3**·2MeCN·H_2O showing the interweaving chains looking down the crystallographic *c* (left) and *a* (right) axes. Color code: **3a** (*trans*), black; **3b** (*cis*) red or green. Hydrogen atoms, solvent molecules and *tert*-butyl groups omitted for clarity.

The cobalt centers in all compounds exhibit very slightly distorted octahedral coordination geometries, with SHAPE indices in the range 0.057-0.15 (Table 2),[47] where the SHAPE indices are based on continuous shape measures such that the closer the index is to zero, the closer the coordination geometry is to the ideal polyhedron. The Co–O and Co–N bond distances for all complexes (Table 2) are in the ranges 1.855(3)–1.911(3) and 1.926(3)–1.992(4) Å, respectively which is consistent with Co(III) centers at the temperature of data collection.[11, 41-48] The bond lengths within the dioxolene ligands are indicative of the oxidation state of the ligand. The C-O bond lengths for complexes **1** and **2** in compounds **1**·2H_2O, **1**·2MeCN·2H_2O, **2**·2EtOH are similar and in the range 1.313(6)-1.344(6) Å (Table 2), which is intermediate between the typical catecholate and semiquinonate values of 1.33-1.39 and 1.27-1.31 Å, respectively. Similarly the (O)C–C(O) bond lengths are in the range 1.411(7)-1.463(8) Å (Table 2), intermediate between the values 1.36-1.44 and 1.45-1.48 Å observed for catecholates and semiquinonates, respectively. A more detailed method proposed by Brown in 2012 to determine oxidation state of dioxolene ligands utilises the C-O and all of the ring C-C bonds to calculate a "Metrical Oxidation State" (MOS), which correlates with the valence of the dioxolene ligand.[49] The

calculated MOS values for **1**·2H_2O, **1**·2MeCN·2H_2O, **2**·2EtOH lie in the range 1.40-1.68 (Table 2). Thus all of the structural data for the 3,5-dbdiox ligands for complexes **1** and **2** in compounds **1**·2H_2O, **1**·2MeCN·2H_2O, **2**·2EtOH are consistent with crystallographic disorder of an equal mixture of the catecholate and semiquinonate forms. It is to be noted that for compounds **1**·2H_2O, **1**·2MeCN·2H_2O and **2** both dioxolene ligands bound to each cobalt center are related by symmetry, while for both *trans* and *cis* chain complexes **3a** and **3b** in compound **3**·2MeCN·H_2O, the 3,5-dbdiox ligands on each cobalt center are not symmetry related and exhibit different bond lengths (Table 2). Although there is still disorder of the catecholate and semiquinonate ligands, the MOS pairs of 1.38, 1.72 and 1.13, 1.91 for **3a** and **3b**, respectively, suggest one ligand has more catecholate character and the other more semiquinonate, particularly for the **3b**. In summary, at the measured temperatures of 130 or 100 K for complexes **1**, **2**, **3a** and **3b** in **1**·2H_2O, **1**·2MeCN·2H_2O, **2**·2EtOH and **3**·2MeCN·H_2O can all be formulated as comprised of {Co^{III}(3,5-dbcat)(3,5-dbsq)} moieties linked by the bis-pyridyl ligands.

Table 2. Selected interatomic distances (Å) and calculated metrical oxidation state (MOS) for **1**·2H$_2$O, **1**·2MeCN·2H$_2$O, **2**·2EtOH and **3**·2MeCN·H$_2$O

Distance (Å) / Parameter	**1**·2H$_2$O	**1**·2MeCN·2H$_2$O	**2**·2EtOH	**3**·2MeCN·H$_2$O	
				3a (*trans*)	**3b** (*cis*)
Co···Co[a]	13.22	13.13	12.80	12.62	11.82
Co···Co[b]	8.09	11.85	7.32	8.03[f]	8.03[f]
Co–O	1.868(3)-1.889(3)	1.886 (2)	1.871(4)-1.889(3)	1.868(3)-1.911(3)	1.855(3)-1.903(4)
Co–N	1.941(4)-1.992(4)	1.945(2)	1.926(3), 1.928(4)	1.942(4), 1.943(4)	1.956(4),1.971(4)
O–C	1.327(5)-1.345(5)	1.325(3), 1.327(3)	1.313(6)-1.332(6)	1.304(6)-1.338(6)	1.291(6)-1.357(5)
C$_a$–C$_b$ [c]	1.410(6), 1.439(6)	1.424(3)	1.463(8), 1.426(7)	1.423(7), 1.427(7)	1.414(6), 1.443(6)
C$_b$–C$_c$, C$_a$-C$_f$ [c]	1.362(6)-1.406(6)	1.400(3), 1.423(3)	1.380(8)-1.416(8)	1.403(7)-1.429(6)	1.383(7)-1.439(6)
C$_c$–C$_d$, C$_e$-C$_f$ [c]	1.370(6)-1.391(6)	1.387(3), 1.389(3)	1.365(8)-1.394(9)	1.375(7)-1.409(8)	1.372(7)-1.407(7)
C$_d$-C$_e$ [c]	1.414(6), 1.427(6)	1.417(3)	1.405(9), 1.409(9)	1.389(9), 1.405(8)	1.397(7), 1.437(7)
MOS [d]	-1.57, -1.68	-1.50	-1.40, -1.52	-1.38, -1.74	-1.13, -1.91
SHAPE Index (O_h) [e]	0.110, 0.143	0.065	0.057, 0.070	0.081	0.150

[a] Intrachain distance. [b] Closest interchain distance. [c] See Chart 2 for labelling of dioxolene positions. [d] Metrical Oxidation State.[49] [e] The closer the index to zero, the less distortion from O_h symmetry.[47] [f] Interchain distance between *cis* and *trans* chains.

Chart 2. Atom labelling for dioxolene ligands.

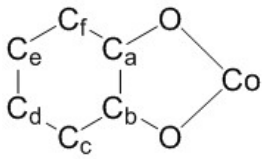

Thermogravimetric Analysis. The thermogravimetric data for compounds **1**, **1**·1.5MeCN·2H_2O, **2**·2EtOH and **3**·MeCN·H_2O were measured between 298 K and 700 K under constant N_2 flow (Figure S3). Compound **1** exhibits no mass loss up to the onset of decomposition around 440 K, which is consistent with a solvent-free composition. In contrast, **1**·1.5MeCN·2H_2O loses mass immediately upon exposure to the N_2 flow, due to rapid desolvation. For **1**·1.5MeCN·2H_2O, the initial mass loss of 7.0 % up to 360 K is in agreement with the 7.9 % required to lose 1.5 MeCN solvate molecules, with the rapid rate of desolvation suggesting that some MeCN is lost immediately as the sample is exposed to nitrogen flow before the heating commences. A plateau between 370 and 420 K may correspond to a putative "**1**·2H_2O" species, before decomposition at higher temperatures. Compound **2**·2EtOH exhibits no mass loss up to 420 K in nitrogen flux, indicating no desolvation in the temperature range of the magnetic measurements (see later). A mass loss of around 8 % between 420 and 470 K may be attributed to partial loss of the EtOH solvate molecules (loss of two EtOH molecules would correspond to 12 %), before decomposition above 510 K. For compound **3**·MeCN·H_2O desolvation is gradual and the initial mass loss of 2.8 % up to 450 K is in good agreement with the loss of a single MeCN molecule, before decomposition at higher temperatures.

Infrared Spectroscopy. Infrared spectra were obtained for compounds **1**, **1**·1.5MeCN·2H_2O, **2**·2EtOH and **3**·MeCN·H_2O as pressed KBr disks (Figure S4). Bands characteristic of the ν(CN) stretching mode for the bis-pyridyl linking ligands are evident

between 1600 and 1614 cm^{-1}. The slight shift from the frequency observed for the free ligand (1597 cm^{-1} for 1,2-bpe, 1587 cm^{-1} for azpy , 1605 cm^{-1} for 1,3-bpp) confirms the coordination to the metal ion.[50] Other bands in the spectra of the cobalt complexes that are also observed in the spectra of the free ligands are in the ranges: 826-837 and 548-576 cm^{-1}. Dioxolenes typically display two groups of medium to strong bands between 1250 and 1650 cm^{-1} associated with C-O stretching modes. The spectra of compounds **1**, **1**·1.5MeCN·2H_2O, **2**·2EtOH and **3**·MeCN·H_2O all exhibit bands in the ranges 1442-1446 cm^{-1} and 1284-1288 cm^{-1}, associated with 3,5-dbcat, as well as bands in the ranges 1461-1465 cm^{-1} and 1357-1356 cm^{-1} due to 3,5-dbsq, suggesting that the dioxolenes ligands are present in both oxidation states in all compounds at room temperature.[41]

Electronic Spectroscopy. Ultra violet-visible diffuse reflectance spectra were obtained on ground samples of **1**, **1**·1.5MeCN·2H_2O, **2**·2EtOH and **3**·MeCN·H_2O at room temperature (Figure S5). All compounds exhibit bands for both chromophores present at room temperature.[51,52] A broad band centered at 730 nm in all four spectra is assigned to a ligand to metal charge transfer (LMCT) transition of a Co(III)-catecholato chromophores. Shoulders between 400 and 450 nm can be attributed to d-d transitions ($^1A_{1g} \rightarrow {}^1T_{1g}$) for low spin octahedral Co(III) complexes. The spectral pattern between 500 and 700 nm observed for compounds **1**, **1**·1.5MeCN·2H_2O, and **3**·MeCN·H_2O is suggestive of Co(II)-semiquinonato chromophores and d $\rightarrow$ π^* metal to ligand charge transfer (MLCT) transitions. In contrast, the spectrum for compound **2**·2EtOH does not clearly show the band characteristic of Co(II), which is due to overlap with the band centered at 480 nm, assigned to n $\rightarrow$ π^* transitions of the azpy ligand.

Magnetic Measurements. Magnetic susceptibility data (Figure 4) were obtained for compounds **1**, **1**·1.5MeCN·2H_2O, **2**·2EtOH and **3**·MeCN·H_2O between 2 and 370 K. Multiple heating-cooling cycles were measured in each case. For reference, the expected low temperature $\chi_m T$ value for a {ls-Co^{III}(3,5-dbcat)(3,5-dbsq)} moiety is 0.38 $cm^3mol^{-1}K$, while high temperature values up to 3.75 $cm^3mol^{-1}K$ are typically observed for uncoupled *hs*-Co^{II} ion and two semiquinonato radicals belonging to the {*hs*-Co^{II}(3,5-dbsq)$_2$} species.[51,53]

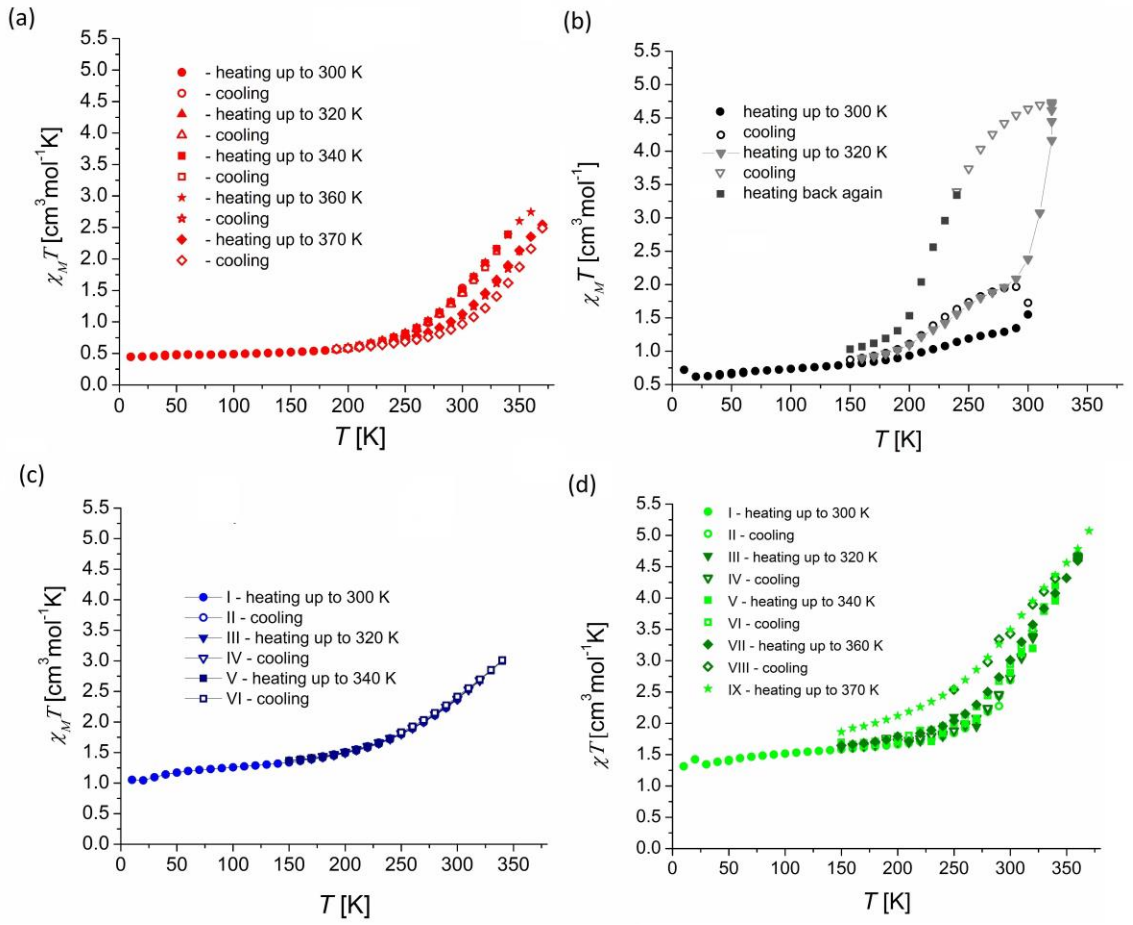

Figure 4. Plots of $\chi_m T$ vs T for (a) **1**, (b) **1**·1.5MeCN·2H_2O, (c) **2**·2EtOH and (d) **3**·MeCN·H_2O. For **3**·MeCN·H_2O, values are reported for two moles given the presence of two structurally different molecules.

Magnetic susceptibility data for **1** were measured in five heating-cooling cycles: from 10 K to 300 K and from 190 K to 320 K, 340 K, 360 K and 370 K (Figure 4). In the first cycle the value of $\chi_m T$ increases gradually from 0.43 $cm^3mol^{-1}K$ up to 0.48 $cm^3mol^{-1}K$ at 200 K, before rapidly increasing to 1.49 $cm^3mol^{-1}K$ at 300 K, indicating the onset of the VT transition. The following cooling restores the same curve. Throughout three next heating cycles (heating to 320 K, 340 K and 360 K, respectively) the $\chi_m T$ profile follows the previously measured curve up to 300 K and then continues increasing, to eventually reach a value of 2.47 $cm^3mol^{-1}K$ in 360 K. Upon cooling down from 360 K the compound unusually exhibits a decrease in the $\chi_m T$ product after heating, which is contrary to all the other previously reported Co-dioxolene based VT systems. [41,56] Since polymorph **1** is completely solvent free and no mass loss is observed in the thermogravimetric profile below 430 K, we attribute this behavior to a thermally driven structural rearrangement.[57,58] Temperature-dependent powder X-ray diffraction confirms that structural rearrangement is taking place at this temperature, with position of two major peaks varying following a thermal hysteresis cycle, and an extra peak appearing above 393 K (Figure S6)

Magnetic susceptibility data were also obtained for partially desolvated **1**·1.5MeCN·2H_2O. In the first heating-cooling cycle the $\chi_m T$ value increases from *ca.* 0.61 $cm^3mol^{-1}K$, firstly gradually to 0.93 $cm^3mol^{-1}K$ in 200 K and the more abruptly to 1.53 $cm^3mol^{-1}K$ at 300 K, which indicates the beginning of the VT transition. The cooling process does not restore the curve, suggesting that the process of losing solvent molecules starts below 300 K, consistent with the thermogravimetric analysis (Figure S3). Subsequent heating to 320 K leads to further desolvation. The $\chi_m T$ product follows the previous profile up to 200 K and then rises sharply to finally reach a value of 4.72 $cm^3mol^{-1}K$ at 320 K. Additional cooling-heating cycles

(Figure S7) afford $\chi_m T$ reaching a plateau at *ca.* 5.1 $cm^3mol^{-1}K$ after heating the sample to 360 K, with no change in the curve upon further cooling or heating. This is consistent with the thermogravimetric analysis (Figure S3) and indicates no further desolvation up to 360 K beyond the putative partially desolvated "**1**·2H_2O" species suggested by thermogravimetric analysis. The shift of the VT transition toward the {*hs*-Co^{II} (3,5-dbsq)$_2$} species after desolvation has been further demonstrated by comparing room temperature X-band EPR spectra (Figure S8) of solvated **1**·1.5MeCN·2H_2O before and after heating at 360 K to partially desolvate the sample. Both species exhibit a sharp signal at g = 2.007, originating from the S = 1/2 semiquinonate radical of the {*ls*-Co^{III}(3,5-dbcat)(3,5-dbsq)} tautomer. However, the signal is much more intense (*ca.* 20 times after double integration of the EPR line and sample mass rescaling) for the solvated sample, the observed intensity difference being consistent with a higher degree of VT interconversion for the heated sample than for the *as synthesized* one.[41] Indeed, as the VT conversion proceeds, the radical signal decreases in intensity due to decreasing fraction of {*ls*-Co^{III}(3,5-dbcat)(3,5-dbsq)} tautomer and the concurrent formation of the {*hs*-Co^{II}(3,5-dbsq)$_2$} one, which is EPR silent at room temperature because of the fast relaxation induced by *hs*-Co(II).[59] This behavior is likely due to the larger volume available for the expansion accompanying the VT transition following partial solvent loss.

The unusually high $\chi_m T$ values following partial desolvation of **1**·1.5MeCN·2H_2O at 340 K and above require some further comments. These can only be justified assuming a complete VT transition to a {*hs*-Co^{II}(3,5-dbsq)$_2$} charge distribution, involving a relatively strong ferromagnetic coupling between the *hs*-Co(II) center and the two radical semiquinonate ligands. It has indeed been suggested on the basis of DFT calculations that, for a *trans*- disposition of the pyridyl ligands around the cobalt centers, ferromagnetic coupling might be observed.[54] Recently,

a high $\chi_m T$ value of around 4.8 $cm^3\ mol^{-1}\ K$ at 200 K has been reported for the high temperature valence tautomer of the mononuclear complex [*trans*-Co(3,5-dbdiox)$_2$(4-Br-Py)$_2$] (4-Br-Py = 4-bromopyridine),[10] which might be due to such ferromagnetic coupling. The *trans*-disposition of the pyridyl ligands results in a local D_{2h} symmetry at the Co(II) centers, providing only one possible antiferromagnetic path through the d_{xz} magnetic orbital (transforming as b_{2g} in D_{2h}), and two ferromagnetic paths, involving d_{z2} and d_{x2-y2}, which are strictly orthogonal to the ligand π^* type magnetic orbitals, resulting in a net ferromagnetic interaction. In agreement with this interpretation, ferromagnetic exchange coupling values in the range 84-263 cm^{-1}, depending on the functional used, have been recently calculated by DFT for a complex with structural and chemical features similar to those of **1**,.[54] If we assume an exchange coupling constant J = 150 cm^{-1} ($\hat{H} = -J(\mathbf{S}_{Co}\cdot\mathbf{S}_{SQ1} + \mathbf{S}_{Co}\cdot\mathbf{S}_{SQ2})$), $g_{Co} = 2.6$ and $g_{SQ} = 2.00$, this would result in a calculated $\chi_m T$ value of 5.2 $cm^3\ mol^{-1}\ K$ at 340 K, thus completely in line with the values observed for **1** after desolvation. This system can thus be considered as a rare example of a ferromagnetically coupled {*hs*-Co^{II}(3,5-dbsq)$_2$} species. Unfortunately, crystallinity of the sample is not maintained upon heating, so it is impossible to determine the bond angles and lengths associated with the cobalt center after heating and desolvation. However prior to desolvation, the SHAPE index determined at 130 K for the cobalt(III) ion in **1**·2MeCN·2H_2O is 0.065 (Table 2), which indicates only very slight deviation from the ideal octahedral coordination geometry that would be required for ferromagnetic coupling in the high temperature valence tautomer.

The low temperature $\chi_m T$ value of 0.98 $cm^3 mol^{-1} K$ for **2**·2EtOH at 10 K suggests the existence of a non-converting *hs*-Co(II)-containing phase, as has been observed previously for other VT complexes.[11,40,56,60] This is consistent with MOS parameters that are slightly closer to the value characteristic of semiquinonate rather than catecholate states (Table 2). Three heating-

cooling cycles (up to 300 K, 320 K and 340 K, respectively) show a reversible, incomplete VT transition with the highest recorded $\chi_m T$ value of 3.00 $cm^3mol^{-1}K$ at 340 K. Full reversibility suggests no solvent loss below 340 K, which is consistent with the thermogravimetric data (Figure S3). The magnetic properties of **2**·2EtOH differ from those reported recently by Tao *et al*. for **2**·2MeCN·2H_2O, which exists in the {*ls*-Co^{III}(3,5-dbsq)(3,5-dbcat)} at low temperatures and then exhibits a complete thermally-induced VT transition associated with desolvation. These differences highlight the role of solvent molecules within the crystalline network in governing the temperature and character of the electronic interconversion.

The low temperature $\chi_m T$ value of 1.31 $cm^3\ mol^{-1}K$ for compound **3**·MeCN·H_2O, calculated per two independent cobalt centers, again shows the presence of a non-negligible quantity of a *hs*-Co(II)-containing phase. The magnetic susceptibility data were measured in four heating-cooling cycles: from 10 K to 300 K and from 190 K to 320 K, 340 K, 360 K and 370 K (Figure 4). The process of desolvation starts above 320 K, as indicated by a small shift in the transition temperature to lower values after heating above this temperature. With each heating-cooling cycle the transition temperature shifts even more, to finally become reversible after heating to 360 K. A detailed analysis of the VT transition has been performed for this sample by plotting the first derivative of the curve for the initial (solvated sample) and final (desolvated sample) heating cycle (Figure 5). The profile of both $d\chi_M T/dT$ curves suggests a VT transition at *ca*. 300 K, while the onset of a second transition above 350 K is evident from the first derivative curve in the final heating cycle. The existence of two distinct thermally induced VT processes has been previously achieved in molecular materials through the presence of crystallographically inequivalent interconverting molecules in the lattice,[60, 61] or arising from weak electronic coupling between VT moieties in dinuclear Co-dioxolene systems. [57, 62, 63] In the present case,

such behavior is most likely due to the existence of two non-equivalent 1D chains, with *cis* and *trans* disposition of pyridyl ligands around cobalt centers, which results in different relative stabilities of the two tautomers.[54]

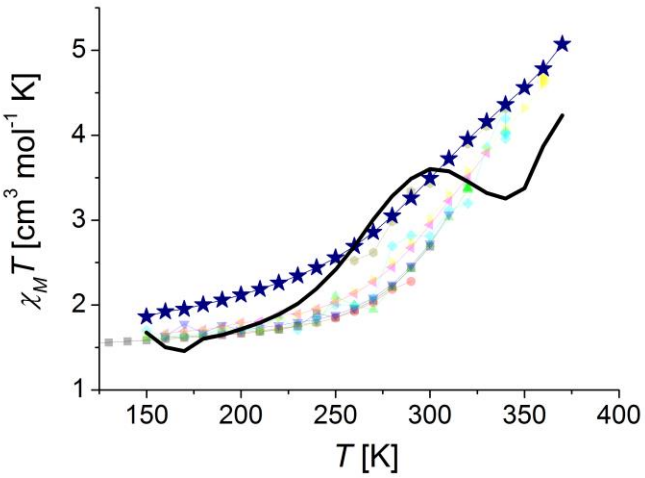

Figure 5. Plot of $\chi_m T$ vs T (scatter points) for the heating cycles for **3**·MeCN·H_2O as per Figure 5(d), and first derivative of the final heating cycle (line, arbitrary units).

Photomagnetic Measurements. To date, photo-induced VT intraconversions have been reported for three VT CPs based on Co-dioxolene units and pyridyl linkers.[39,40,64] As all four compounds in the present work exhibit thermally-induced VT transitions, all were also investigated for light-induced transitions. Following irradiation with the 532 nm wavelength light at 10 K, an immediate increase of the $\chi_m T$ product is evident for **1**, **1**·1.5MeCN·2H_2O, **2**·2EtOH and **3**·MeCN·H_2O, which indicates a photoinduced VT transition (Figure 6). The initial conversion rates are in the range 10-17 %, which is comparable with many literature Co-bis dioxolene VT complexes.[65] This behavior can be attributed to sample opacity and incomplete penetration of the laser light or to the significant energy difference between the ground state {*ls*-

Co^{III}(3,5-dbcat)(3,5-dbsq)} and photoinduced metastable {*hs*-Co^{II}(3,5-dbsq)$_2$} one, as suggested by the high temperature of thermal VT transition of the chains.[66] After the laser was switched off and the samples warmed at a rate of 0.3 K min^{-1}, the $\chi_m T$ values increase further, due to the non-Curie nature of the photo-induced *hs*-Co(II) ion, to finally decrease and meet the non-irradiated profiles. The temperatures at which the thermal susceptibility curves rejoins the non-irradiated profiles, stated in Table 3 as effective T_{LIESST} (LIESST = light induced excited spin state trapping), are in range of 55 to 65 K, consistent with values reported for other VT complexes (38–80 K).[67] For **3**·MeCN·H_2O only one distinct photo-induced transition is observed, in contrast to the thermal data, either because irradiation at low temperature does not activate the second interconversion entirely or the relaxation parameters of the two chains are similar and cannot be resolved on the timescale of the magnetic measurements.

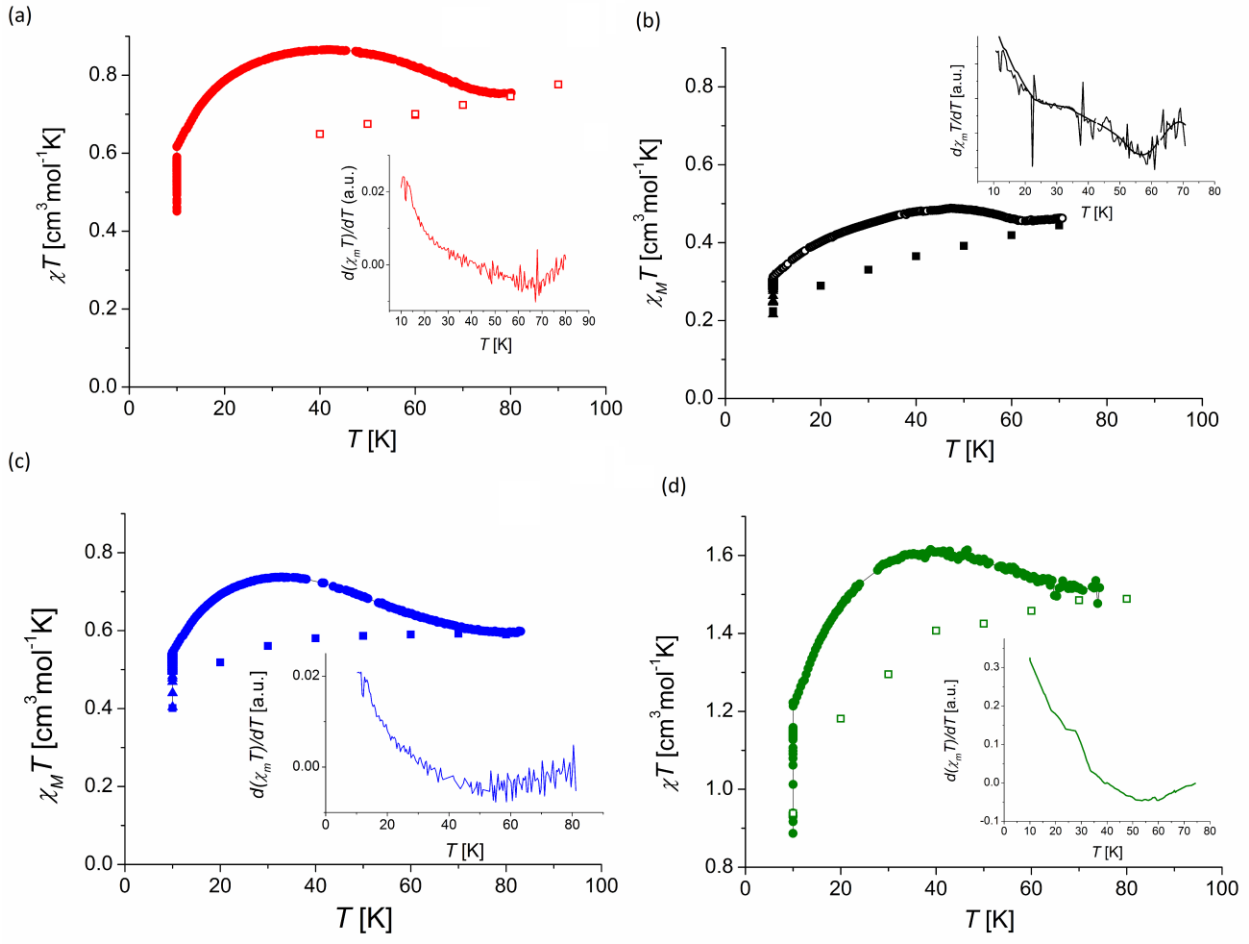

Figure 6. Plot of $\chi_m T$ versus T for the photo-induced VT transitions for (a) **1**, (b) **1**·1.5MeCN·2H_2O, (c) **2**·2EtOH and (d) **3**·MeCN·H_2O. Insets: Plot of d($\chi_m T$)/dT versus T for the LIESST branch, the minimum used to evaluate the effective T_{LIESST}.

Table 3. Conversion rates and T_{LIESST} parameters for photo-induced VT transitions in **1**, **1**·1.5MeCN·2H_2O, **2**·2EtOH and **3**·MeCN·H_2O.

	1	**1**·1.5MeCN·2H_2O	**2**·2EtOH	**3**·MeCN·H_2O
Conversion rate (%)	17	10	14	12
Effective T_{LIESST} (K)	65	57	55	56

CONCLUDING REMARKS

Four new polymeric VT compounds have been synthesized and characterized by single crystal X-ray diffraction TGA, IR, UV-Vis and magnetic studies; one of these is a differently solvated form of a previously reported complex. All compounds undergo a thermally-driven VT transition, the characteristics of which are affected by the choice of linking bis-pyridyl ancillary ligand and the degree of solvation. The role of solvation is particularly evident from the comparison of the behavior of two differently solvated forms of $[Co(3,5\text{-dbdiox})_2(1,2\text{-bpe})]_\infty$ (**1**). Compound **1**, crystallizing from an ethanol/water mixture, contains highly disordered and readily lost hydrate molecules. Upon heating, crystallites of **1** undergo a thermally-induced structural rearrangement, which, unusually, shifts the VT transition to higher temperatures. Crystallization from acetonitrile instead affords **1**·2MeCN·2H_2O, which exhibits a strongly solvent-dependent VT conversion with a remarkably high final magnetic susceptibility value which we attribute to a relatively strong ferromagnetic coupling between the *hs*-Co(II) center and the two semiquinonate radicals formed after the VT transition. On the other hand, compound **2**·2EtOH exhibits a gradual increase in the $\chi_m T$ versus T curve and no desolvation in the measured temperature range. Lastly, compound **3**·2MeCN·H_2O is, to the best of our knowledge, the first example of VT coordination polymer containing two individual 1D chains in the structure, which are geometric isomers of each other; one exhibiting a *cis* and the other a *trans* disposition of the N-donor ligands with respect to the $\{Co(3,5\text{-dbdiox})_2\}$ unit, resulting in a two-step temperature driven VT tautomeric transition in the complex, previously unreported in a VT coordination polymer. Moreover, all four compounds also exhibit the possibility of photo-induction of the VT

conversion in the solid state, even if the observed conversion rates of 10-17 % indicate only a partial conversion. Overall, this work illustrates the potential of cobalt bis-dioxolene units as robust building blocks for the construction of polymeric systems with thermally and optically controllable electronic states. Ultimately strong intramolecular ferromagnetic interactions and the presence of inequivalent molecular chains in the solid state may give rise to multistable high spin systems. Furthermore, the synthetic procedure established in this work should be equally applicable to divergent polydentate ligands of denticity greater than two, opening a route to 2D and 3D VT CPs. This is particularly interesting since only a single VT CP of dimensionality higher than one has been reported to date,[64] and higher dimensional VT CPs are particularly promising for achieving enhanced cooperativity of the VT transition, as well as for transferring the VT properties to more technologically convenient platforms such as gels, films and nanoparticles for future applications in devices.

ASSOCIATED CONTENT

Supporting Information.

X-ray crystallographic files in CIF format for **1**·2H_2O, **1**·2MeCN·2H_2O, **2**·2EtOH and **3**·2MeCN·H_2O. Additional structural figures, thermogravimetric analysis data, ultra-violet-visible diffuse reflectance spectra, powder X-ray diffraction data and EPR spectra. This material is available free of charge via the Internet at http://pubs.acs.org.

AUTHOR INFORMATION

Corresponding Authors

*E-mail: c.boskovic@unimelb.edu.au, lorenzo.sorace@unifi.it

Notes

The authors declare no competing financial interest.

ACKNOWLEDGMENT

We thank the Australian Research Council for financial support to CB and LS. Part of this research was undertaken on the MX1 and MX2 beamlines at the Australian Synchrotron, Victoria, Australia. GP and LS acknowledge financial support from the European Research Council through the Advanced Grant "MolNanoMas" (267746) and from Ente Cassa di Risparmio di Firenze.

REFERENCES

(1) *Spin-Crossover Materials*; Halcrow, M. A., Ed.; John Wiley & Sons Ltd: Chichester, 2013, entire volume.

(2) Dunbar, K. R.; Achim, C.; Shatruk, M. In *Spin-Crossover Materials - Properties and Applications*; John Wiley & Sons Ltd: Chichester, 2013; pp 171–202.

(3) Hendrickson, D. N.; Pierpont, C. G. *Top. Curr. Chem.* **2004**, *1*, 63.

(4) Dei, A.; Gatteschi, D.; Sangregorio, C.; Sorace, L. *Acc. Chem. Res.* **2004**, *37*, 827.

(5) Evangelio, E.; Ruiz-Molina, D. *Eur. J. Inorg. Chem.* **2005**, *2005*, 2957.

(6) Tezgerevska, T.; Alley, K. G.; Boskovic, C. *Coord. Chem. Rev.* **2014**, *268*, 23.

(7) Buchanan, R. M.; Pierpont, C. G. *J. Am. Chem. Soc.* **1980**, *102*, 4951.

(8) Bauer, W.; Lochenie, C.; Weber, B. *Dalton Trans.* **2014**, *43*, 1990.

(9) Sciortino, N. F.; Scherl-Gruenwald, K. R.; Chastanet, G.; Halder, G. J.; Chapman, K. W.; Létard, J.-F.; Kepert, C. J. *Angew. Chem. Int. Ed. Engl.* **2012**, *51*, 10154.

(10) Schmidt, R. D.; Shultz, D. A; Martin, J. D.; Boyle, P. D. *J. Am. Chem. Soc.* **2010**, *132*, 6261.

(11) Schmidt, R. D.; Shultz, D. A; Martin, J. D. *Inorg. Chem.* **2010**, *49*, 3162.

(12) Tao, J.; Maruyama, H.; Sato, O. *J. Am. Chem. Soc.* **2006**, *128*, 1790.

(13) Munoz, M. C.; Real, J. A. In *Spin-Crossover Materials - Properties and Applications*; John Wiley & Sons Ltd: Chichester, 2013; pp 121–170.

(14) Koningsbruggen van, P. J. *Top. Curr. Chem.* **2004**, *233*,123.

(15) Murray, K. S.; Kepert, C. J. *Top. Curr. Chem.* **2004**, *233*, 195.

(16) Real, J. A.; Gaspar, A. B.; Muñoz, M. C. *Dalton Trans.* **2005**, 2062.

(17) Muñoz, M. C.; Real, J. a. *Coord. Chem. Rev.* **2011**, *255*, 2068.

(18) Gutlich, P.; Goodwin, H. I *Top. Curr. Chem.* **2004**, *233*, 1.

(19) Rubio, M.; Hernández, R.; Nogales, A.; Roig, A.; López, D. *Eur. Polym. J.* **2011**, *47*, 52.

(20) Seredyuk, M.; Gaspar, A. B.; Ksenofontov, V.; Reiman, S.; Galyametdinov, Y.; Haase, W.; Rentschler, E.; Gütlich, P. *Chem. Mater.* **2006**, *18*, 2513.

(21) Fujigaya, T.; Jiang, D. L.; Aida, T. *J. Am. Chem. Soc.* **2005**, *127*, 5484.

(22) Roubeau, O.; Natividad, E.; Agricole, B.; Ravaine, S. *Langmuir* **2007**, *23*, 3110.

(23) Forestier, T.; Kaiba, A.; Pechev, S.; Denux, D.; Guionneau, P.; Etrillard, C.; Daro, N.; Freysz, E.; Létard, J. F. *Chem. Eur. J.* **2009**, *15*, 6122.

(24) Faulmann, C.; Chahine, J.; Malfant, I.; de Caro, D.; Cormary, B.; Valade, L. *Dalton Trans.* **2011**, *40*, 2480.

(25) Forestier, T.; Mornet, S.; Daro, N.; Nishihara, T.; Mouri, S.; Tanaka, K.; Fouché, O.;

Freysz, E.; Létard, J.-F. *Chem. Commun.* **2008**, 4327.

(26) Fouché, O.; Degert, J.; Jonusauskas, G.; Daro, N.; Létard, J.-F.; Freysz, E. *Phys. Chem. Chem. Phys.* **2010**, *12*, 3044.

(27) GalÍ, G.; Deldicque, D.; Degert, J.; Forestier, T.; Ĺtard, J. F.; Freysz, E. *Appl. Phys. Lett.* **2010**, *96*, 4.

(28) Aromí, G.; Barrios, L.; Roubeau, O.; Gamez, P. *Coord. Chem. Rev.* **2011**, *255*, 485.

(29) Bauer, W.; Dîrtu, M. M.; Garcia, Y.; Weber, B. *CrystEngComm* **2012**, *14*, 1223.

(30) Bao, X.; Guo, P. H.; Liu, J. L.; Leng, J. D.; Tong, M. L. *Chem. Eur. J.* **2011**, *17*, 2335.

(31) Bao, X.; Liu, J.-L.; Leng, J.-D.; Lin, Z.; Tong, M.-L.; Nihei, M.; Oshio, H. *Chemistry* **2010**, *16*, 7973.

(32) Ohba, M.; Yoneda, K.; Agusti, G.; Muñoz, M. C.; Gaspar, A. B.; Real, J. a.; Yamasaki, M.; Ando, H.; Nakao, Y.; Sakaki, S.; Kitagawa, S. *Angew. Chemie Int. Ed.* **2009**, *48*, 4767.

(33) Southon, P. D.; Liu, L.; Fellows, E. A.; Price, D. J.; Halder, G. J.; Chapman, K. W.; Moubaraki, B.; Murray, K. S.; Létard, J. F.; Kepert, C. J. *J. Am. Chem. Soc.* **2009**, *131*, 10998.

(34) Jung, O.; Pierpont, C. G. *J. Am. Chem. Soc.* **1994**, *116*, 2229.

(35) Bodnar, S. H.; Caneschi, A.; Dei, A.; Shultz, D. A.; Sorace, L. *Chem. Commun.* **2001**, *2001*, 2150.

(36) Beni, A.; Dei, A.; Shultz, D.; Sorace, L. *Chem. Phys. Lett.* **2006**, *428*, 400.

(37) Imaz, I.; Maspoch, D.; Rodríguez-Blanco, C.; Pérez-Falcón, J. M.; Campo, J.; Ruiz-Molina, D. *Angew. Chem. Int. Ed. Engl.* **2008**, *47*, 1857.

(38) Guardingo, M.; Busqué, F.; Novio, F.; Ruiz-Molina, D. *Inorg. Chem.* **2015**, *54*, 6776.

(39) Chen, L.; Wei, R.; Tao, J.; Huang, R.; Zheng, L. *Sci. China Chem.* **2012**, *55*, 1037.

(40) Chen, X.; Wei, R.; Zheng, L.; Tao, J. *Inorg. Chem* **2014**, *53*, 13212.

(41) Mulyana, Y.; Poneti, G.; Moubaraki, B.; Murray, K. S.; Abrahams, B. F.; Sorace, L.; Boskovic, C. *Dalton Trans.* **2010**, *39*, 4693.

(42) Cheng, W.-Q.; Li, G.-L.; Zhang, R.; Ni, Z.-H.; Wang, W.-F.; Sato, O. *J. Mol. Struct.* **2015**, *1087*, 68.

(43) Agustı, G.; Cobo, S.; Gaspar, A. B.; Szila, P. Á.; Vieu, C.; Mun, M. C.; Real, A.; Bousseksou, A. *Chem. Mater.* **2008**, *20*, 6721.

(44) Dolomanov, O. V.; Bourhis, L. J.; Gildea, R. J.; Howard, J. a K.; Puschmann, H. *J. Appl. Crystallogr.* **2009**, *42*, 339.

(45) Sheldrick, G. M. *Acta Crystallogr. Sect. A Found. Crystallogr.* **2007**, *64*, 112.

(46) van der Sluis, P.; Spek, A. L. *Acta Crystallogr. Sect. A Found. Crystallogr.* **1990**, *46*, 194.

(47) Alvarez, S.; Avnir, D.; Llunell, M.; Pinsky, M. *New J. Chem.* **2002**, *26*, 996.

(48) Pierpont, C. G.; Buchanan, R. M. *Coord. Chem. Rev.* **1981**, *38* (1), 45.

(49) Brown, S. N. *Inorg. Chem.* **2012**, *51*, 1251.

(50) Garcia, H. C.; De Almeida, F. B.; Diniz, R.; Yoshida, M. I.; De Oliveira, L. F. C. *J. Coord. Chem.* **2011**, *64*, 1125.

(51) Beni, A.; Dei, A.; Laschi, S.; Rizzitano, M.; Sorace, L. *Chemistry* **2008**, *14*, 1804.

(52) Tourón Touceda P.; Mosquera Vázquez, S.; Lima, M.; Lapini, A.; Foggi, P.; Dei, A.; Righini, R.; *Phys. Chem. Chem. Phys.* **2012**, *14*, 1038.

(53) Sato, O.; Tao, J.; Zhang, Y.-Z. *Angew. Chem. Int. Ed. Engl.* **2007**, *46*, 2152.

(54) Witt, A.; Heinemann, F. W.; Sproules, S.; Khusniyarov, M. M. *Chem. Eur. J.* **2014**, *20*, 11149.

(55) Gass, I. A.; Tewary, S.; Nafady, A.; Chilton, N. F.; Gartshore, C. J.; Asadi, M.; Lupton, D. W.; Moubaraki, B.; Bond, A. M.; Boas, J. F.; Guo, S. X.; Rajaraman, G.; Murray, K. S. *Inorg. Chem.* **2013**, *52*, 7557.

(56) Poneti, G.; Mannini, M.; Cortigiani, B.; Poggini, L.; Sorace, L.; Otero, E.; Sainctavit, P.; Sessoli, R.; Dei, A. *Inorg. Chem.* **2013**, *52*, 11798.

(57) Juhász, G.; Matsuda, R.; Kanegawa, S.; Inoue, K.; Sato, O.; Yoshizawa, K. *J. Am. Chem. Soc.* **2009**, *131*, 4560.

(58) Alley, K. G.; Poneti, G.; Robinson, P. S. D.; Nafady, A.; Moubaraki, B.; Aitken, J. B.; Drew, S. C.; Ritchie, C.; Abrahams, B. F.; Hocking, R. K.; Murray, K. S.; Bond, A. M.; Harris, H. H.; Sorace, L.; Boskovic, C. *J. Am. Chem. Soc.* **2013**, *135*, 8304.

(59) Beni, A.; Dei, A.; Rizzitano, M.; Sorace, L. *Chem. Commun.* **2007**, 2160.

(60) Kiriya, D.; Chang, H.-C.; Kamata, A.; Kitagawa, S. *Dalton Trans.* **2006**, 1377.

(61) Poneti, G.; Mannini, M.; Sorace, L.; Sainctavit, P.; Arrio, M.-A.; Rogalev, A.; Wilhelm, F.; Dei, A. *Chemphyschem* **2009**, *10*, 2090.

(62) Dapporto, P.; Dei, A.; Poneti, G.; Sorace, L. *Chem. Eur. J.* **2008**, *14*, 10915.

(63) Hearns, N. G. R.; Korcok, J. L.; Paquette, M. M.; Preuss, K. E. *Inorg. Chem.* **2006**, *45*, 8817.

(64) Alley, K. G.; Poneti, G.; Aitken, J. B.; Hocking, R. K.; Moubaraki, B.; Murray, S.; Abrahams, B. F.; Harris, H. H.; Sorace, L.; Boskovic, C.; Murray, K. S. *Inorg. Chem.* **2012**, *51*, 3944.

(65) Li, B.; Chen, L.-Q.; Wei, R.-J.; Tao, J.; Huang, R.-B.; Zheng, L.-S.; Zheng, Z. *Inorg. Chem.* **2011**, *50* , 424.

(66) Sato, O.; Cui, A.; Matsuda, R.; Tao, J.; Hayami, S. *Acc. Chem. Res.* **2007**, *40*, 361.

(67) Hauser, A. *Top. Curr. Chem.* **2004**, *234*, 155.

(68) Boskovic, C. in *Spin-Crossover Materials - Properties and Applications*; John Wiley &

Sons Ltd: Chichester, 2013. 203.

(69) Witt, A.; Heinemann, F. W.; Khusniyarov, M. M. *Chem. Sci.* **2015**, *6,* 4599.

Insert Table of Contents Graphic and Synopsis Here

A family of 1D coordination polymers of formula $[Co(3,5\text{-dbdiox})_2(L)]$ (3,5-dbdiox = 3,5-di-*tert*-butyldioxolene; L = divergent bis-pyridyl linking ligand) exhibit solvation-dependent thermally- and photo-induced valence tautomeric transitions.